Immune surveillance and pruning of neuronal stem cells in the medaka retina

Authors:

Rashi Agarwal[1,2‡], Joergen Benjaminsen[1‡], Katharina Lust[3#], Clara Becker[1#], Natalia Fuchs[1], Eva Hasel de Carvalho[1], Fanny Eggeler[4], Omnia El Said Ibrahim[1], Narges Aghaallaei[5], Baubak Bajoghli[6], Joachim Wittbrodt[1*]

[1] Centre for Organismal Studies, Heidelberg University, Heidelberg, Germany.

[2] Heidelberg Biosciences International Graduate School (HBIGS), Heidelberg, Germany.

[3] Present address: Institute of Molecular Biotechnology (I), Vienna BioCenter (VBC), Vienna, Austria.

[4] Present address: Biozentrum, University of Basel, Basel, Switzerland

[5] Present address: Ludwig Boltzmann Institute for Hematology and Oncology, Medical University of Vienna, University Clinic for Internal Medicine I, Vienna, Austria

[6] Present address: Austrian BioImaging/CMI, Vienna, Austria

[‡] These authors contributed equally to this work

# These authors contributed equally to this work

* Author for correspondence (jochen.wittbrodt@cos.uni-heidelberg.de)

Key words: Retinal stem cells, microglia, phagocytosis, chemokine, medaka

Abstract

Stem cell populations in tissues require precise regulation of their number and quality to maintain proper organ growth and regenerative capacity. Amongst various regulatory mechanisms, immune cells are emerging to directly regulate stem cell populations. The medaka retinal stem cell niche, a model for lifelong neurogenic growth, provides a system to study immune cell-stem cell interactions. Here we investigate how microglia, the resident macrophages of the central nervous system, regulate the retinal stem cell niche. We identify that *bona fide* retinal stem cells express the chemokine ccl25b while its cognate receptor, ccr9a, is expressed in microglia. These microglia form a surveillance ring adjacent to the stem cell niche and actively phagocytose retinal stem cells. Interference with microglia by deletion of *spi1b* reveals that microglia absence leads to increased numbers of ccl25b-positive stem cells and results in morphological defects in the retinal stem cell niche and retina. Targeted mutation of ccl25b specifically affects microglia mobility under injury conditions, however, we did not observe any morphological defects indicating that ccl25b-ccr9a signaling is not essential for stem cell maintenance. Overall, our data show that under homeostatic conditions the retinal stem cell population, essential for proper eye development, is actively pruned by immune surveillance.

Introduction

Stem cell reservoirs are essential for growth, homeostasis, and tissue regeneration in multicellular organisms (Hollyfield, 1971; Johns, 1977; Johns & Easter, 1977). These long-lived cells continuously produce new stem and progenitor cells while resisting cell death (Soteriou & Fuchs, 2018). Their quantity and quality must be precisely regulated to prevent tissue overgrowth and cellular deterioration.

The retinal stem cell (RSC) niche of the teleost medaka (Oryzias latipes) provides a well-established model for studying neuronal stem cells (Centanin et al., 2011) due to medaka's short generation time, ease of genetic manipulation and vast landscape of available transgenic reporter lines. Located in the ciliary marginal zone (CMZ) in a ring around the distal edge of the optic cup, multipotent stem cells sustain lifelong retinal growth (Centanin et al., 2014; Reinhardt et al., 2015; Soteriou & Fuchs, 2018). A population of neuroretinal progenitor cells, located between the stem cell ring and the stratified retina, contains transiently amplifying cells that contribute to both the inner and outer nuclear layers (Tsingos et al., 2019). This distinctive architecture allows reliable identification of multipotent stem cells through lineage tracing experiments (Centanin et al., 2014; Centanin et al., 2011).

Recent evidence suggests that immune cells, particularly tissue-resident macrophages and microglia, extend beyond their classical immune functions to contribute to tissue homeostasis, stem cell regulation, and regeneration (Cunningham et al., 2013; de Almeida et al., 2023; Nath et al., 2024; Ratnayake et al., 2021). In the central nervous system (CNS), microglia are unique among retinal cells as they originate outside the RSC niche, entering the CNS at embryonic stages (E11.5 in mice, 25 hours post fertilization in zebrafish) (Herbomel et al., 2001; Santos et al., 2008).

Traditionally, microglia are known primarily for efferocytosis - the removal of apoptotic cells (Ravichandran, 2011) – and thus contribute to shaping developing tissues. Recently, a "groom or doom" interaction was reported for the hematopoietic stem cell niche of zebrafish and mice during embryogenesis: local macrophages were observed to undergo lengthy interactions with stem cells preceding cell division. These interactions often resulted in either the partial, or complete, phagocytosis of stem cells which did not display markers for apoptosis (Wattrus et al., 2022).

Building on our understanding of the RSC niche organization, we addressed if and how microglia regulate retinal stem cell numbers and contribute to coordinated retinal growth in medaka. Using a newly established retinal stem cell reporter line, we characterize the interactions between RSCs expressing the chemokine ccl25b and microglia expressing its cognate receptor ccr9a.

Unlike the previously established role of ccl25b-ccr9a signaling in the recruitment of lymphocytes in the intestine in mammals and fish(Aghaallaei et al., 2022; Bajoghli, 2013; Uehara et al., 2002), we report a novel function of this chemokine-receptor interaction in the retina. Furthermore, we examine how the complete absence of microglia affects retinal development and growth, providing insights into immune cell-mediated regulation of the retinal stem cell pool.

Results

Ccl25b **chemokine and ccr9a receptor expression in the medaka retina**

RSCs are specifically labelled in a stable transgenic line where a ccl25b regulatory element drives GFP reporter expression (*ccl25b::GFP*). This line was initially generated to follow the dynamics of cells expressing *ccl25b*, a chemokine which is known to be involved in the recruitment of lymphocytes in the intestine (Aghaallaei et al., 2022; Campbell & Butcher, 2002; Sigmundsdottir & Butcher, 2008) and thymus (Baubak Bajoghli, 2009). We detected the expression of *ccl25b* chemokine at the periphery of the ciliary marginal zone (CMZ), partially overlapping with previously described *rx2* expressing retinal stem and progenitor cells (Fig. 1A) (Reinhardt et al., 2015). The endogenous expression of *ccl25b* transcripts in

the RSC zone was validated by *in situ* hybridization chain reaction (HCR) (Fig.1 S1B). To test if *ccl25b* expressing cells indeed represent multipotent retinal stem cells, we used GaudíRSG, an established Cre-LoxP based lineage tracing tool (Centanin et al., 2014). Here, Cre induced recombination will lead to the expression of GFP after the Cre mediated excision of a default DsRed/Stop cassette. We employed the ccl25b regulatory element mentioned above (Aghaallaei et al., 2022) to specifically drive the expression of a hormone inducible Cre recombinase in *ccl25b* expressing cells and established a stable transgenic line in the background of the *GaudíRSG* line. We generated a tamoxifen-inducible *ccl25b::Cre^{ERT2},GaudíRSG* transgenic line and clonally activated colour switches in individual *ccl25b*-positive cells specifically labelling those and all of their descendants. The long-term lineage of *ccl25b*-expressing cells was analysed in fish 6-week post Cre-mediated recombination at hatching stage, GFP expressing clones originating from *ccl25b* expressing cells in the CMZ were analysed via wholemount immunostaining. Lineage analysis revealed that *ccl25b*-positive cells established induced Arched Continuous Stripes, iArCoSs(Centanin et al., 2014), clonal strings originating in the stem cell niche of the CMZ differentiated into all neuroretinal cell types and thus represent neuroretinal stem cells (Fig. 1B). Early induction for 3 days post hatching was also evaluated to validate the clonal capacity of these ccl25b-expressing cells in a short period. As expected, few GFP positive cells were observed in the CMZ for such a short induction time wherein the clone partially overlaps with early retinal progenitor cells expressing rx2 and eventually produces late progenitors (Fig.1 S1E-E'). The proliferative capacity of *ccl25b* expressing RSCs was evaluated with BrdU labelling, showing that these cells are slowly proliferating as they did not incorporate BrdU when exposed for 1 day unlike the adjacent fast-cycling progenitor cells, which show BrdU incorporation (Fig.1 S1D-D'). *ccl25b* based iArCoSs were exclusively detected in the neuroretina. This validates *ccl25b* expressing cells as *bona fide* multipotent neuro-retinal stem cells residing in the peripheral tip of the CMZ.

We complemented our analysis by probing for the presence and localization of cells expressing *ccr9a*, the cognate receptor of *ccl25b* in the retina of young fish at the hatching stage. We used an established transgenic line, *ccr9a::GFP (Bajoghli et al., 2015)* and detected GFP expressing cells around the CMZ and in the INL region of the retina (Fig. 1C). The endogenous expression of *ccr9a* in the retina was confirmed by HCR *in situ* staining. (Fig.1 S1C).

Ccr9a-expressing cells were characterized as immune cells using immunostaining for lymphocyte cytosolic protein 1 (Lcp1) (Jones et al., 1998). Among all Lcp1-positive cells analyzed (n = 316 cells in 56 sections from 4 fish), 97% co-expressed the chemokine receptor ccr9a (Fig. 1C). *Ccr9a*-positive cells were further validated as immune cells by the

co-expression of *cxcr3a::GFP***,** a well-established macrophage-specific marker (Aghaallaei et al., 2010) (Fig. 1D). Under homeostatic conditions, the only immune cells known to colonize the immune-privileged retina are primordial macrophages, which give rise to microglia (Herbomel et al., 1999, 2001).

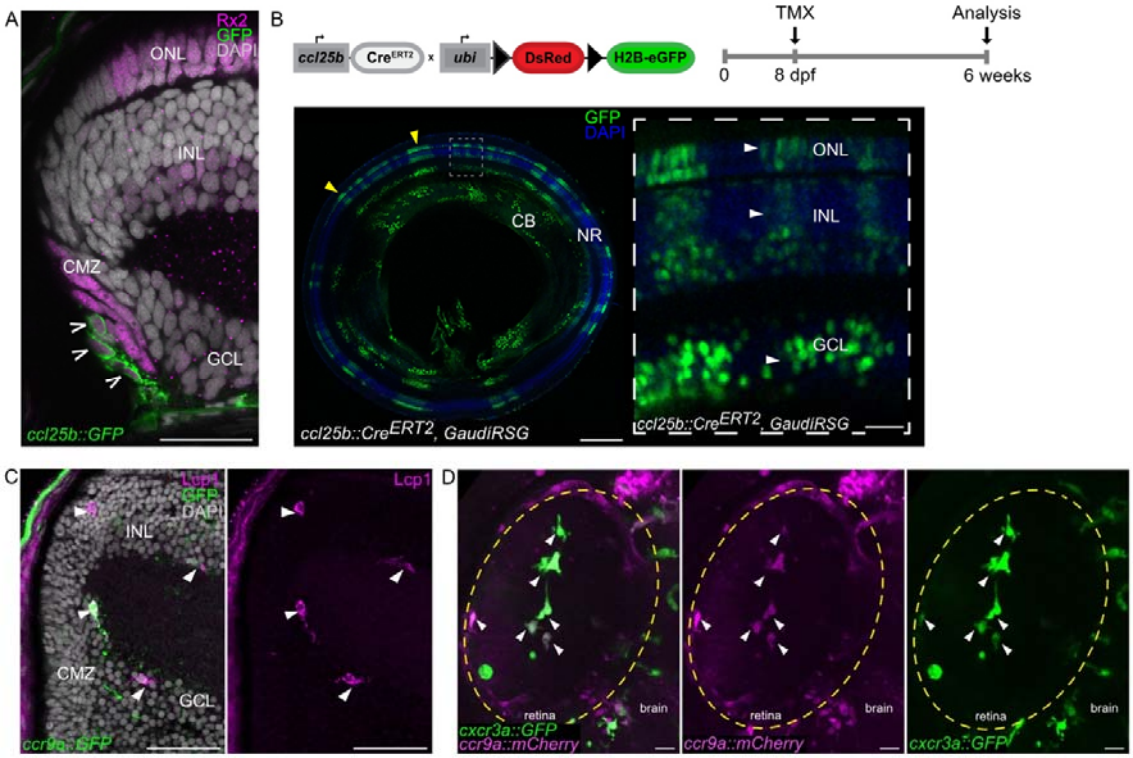

Figure 1: Characterization of *ccl25b* as a retinal stem cell marker and *ccr9a* as marker for microglia in the retina.

(A) Transverse section of a retina derived from a *ccl25b::GFP* reporter hatchling. GFP-positive cells (open arrowheads) are located in the most peripheral cells of the CMZ and the Rx2-positive (magenta) domain, cell nuclei are stained with DAPI (grey). Scale bar: 20 µm. (B) Cre/loxP-mediated lineage tracing of *ccl25b*-positive cells: Genetic construct and induction scheme and wholemount *ccl25b::Cre^{ERT2} X GaudíRSG* retina, where recombination (red to green) was induced at hatching stage and analysed 6 weeks later. GFP-positive clones (iArCoS) (yellow arrowheads) can be detected in the neural retina (NR) and the ciliary body (CB). Scale bar: 200 µm. Zoomed in area of GFP-positive iArCoS (white dashed box) shows GFP+ cells in all neuroretinal layers (white arrowheads) in *ccl25b::Cre^{ERT2} X GaudíRSG* retinae. Scale bar: 20 µm. (C) Transverse section of a *ccr9a::GFP* hatchling retina. GFP positive cells are present in proximity to the CMZ region and in INL region. Lcp1 staining overlaps with *ccr9a::GFP* positive cells (white arrowheads). Cell nuclei are stained with DAPI (grey) Scale bar: 20 µm. (D) Co-expression of the macrophage reporter

cxcr3a::GFP with *ccr9a::mCherry* in embryonic stage retinae (stage 28) as observed by *in vivo* confocal imaging. White arrowheads indicate co-expressing cells. Scale bar: 20 µm.

Retinal stem cells are phagocytosed by tissue resident microglia

To address if there is an immune - stem cell interaction in the retina, we first carried out a detailed analysis of the spatial arrangement of *ccl25b* positive retinal stem cells and microglia expressing the cognate receptor *ccr9a* in the retina of freshly hatched medaka larvae. We carefully analysed 3D reconstructions of retinae of double positive *ccl25b::GFP; ccr9a:RFP* reporter fish. While *ccl25b* expressing RSCs resided in a ring in the very periphery of the CMZ (open arrowheads in Fig. 2A, 3-D schematic), microglia expressing *ccr9a* formed a concentric double ring at the proximal edge of the CMZ close to inner plexiform layer (IPL) and outer plexiform layer (OPL). Each ring composed of evenly spaced *ccr9a*-positive cells contacting each other (Fig. 2A, 3D schematic, Fig.2 Supplementary movie 1). Microglia extend protrusions in various directions and are in direct contact with the *ccl25b* positive RSCs (Fig. 2B).

An important feature of immune cells, particularly macrophages, is their capacity to phagocytose debris, damaged cells and foreign particles(Arandjelovic & Ravichandran, 2015; Nakayama, 2018). To address whether microglia phagocytose *ccl25b*-positive stem cells, we took advantage of the extended stability of red-fluorescent-protein (RFP)-tagged-H2B in the phagosomal compartment (Villani et al., 2019). We used a double transgenic line specifically labelling the nuclei of RSCs with histone-coupled RFP (*ccl25b::H2B-RFP*) and the *ccr9a*-positive immune cells with GFP (*ccr9a::GFP*) (Fig. 2A). We found that GFP-labelled microglia contained RFP-positive phagosomes (Fig. 2C) and quantified the phagocytosis of stem cells by counting the number of microglia containing RFP positive phagosomes. At hatching stage, we detected active uptake by phagocytosis of stem cells in 61 % of the *ccr9a*-positive microglia as indicated by RFP-positive phagosomes (Fig. 3A').

We investigated the dynamics of interactions between RSCs and microglia as well as their phagocytic activity using two-photon *in vivo* imaging at hatching stage. This analysis revealed microglia actively transporting stem cell derived, RFP-positive, phagosomes within the ciliary marginal zone (CMZ) (Fig. 2D, Fig.2 Supplementary movie 2). We observed microglia containing H2B-RFP-positive nuclei within their phagosomes, indicating the uptake of stem cell nuclei (Fig. 2D, asterisk). We next addressed whether the phagocytosed stem cells represent cells being cleared through classical efferocytosis of apoptotic cells. Strikingly, TUNEL staining did not detect any apoptotic cells among RSCs. (Fig.3 S1C). This indicates that the detected prominent phagocytosis of RSCs is independent of apoptosis.

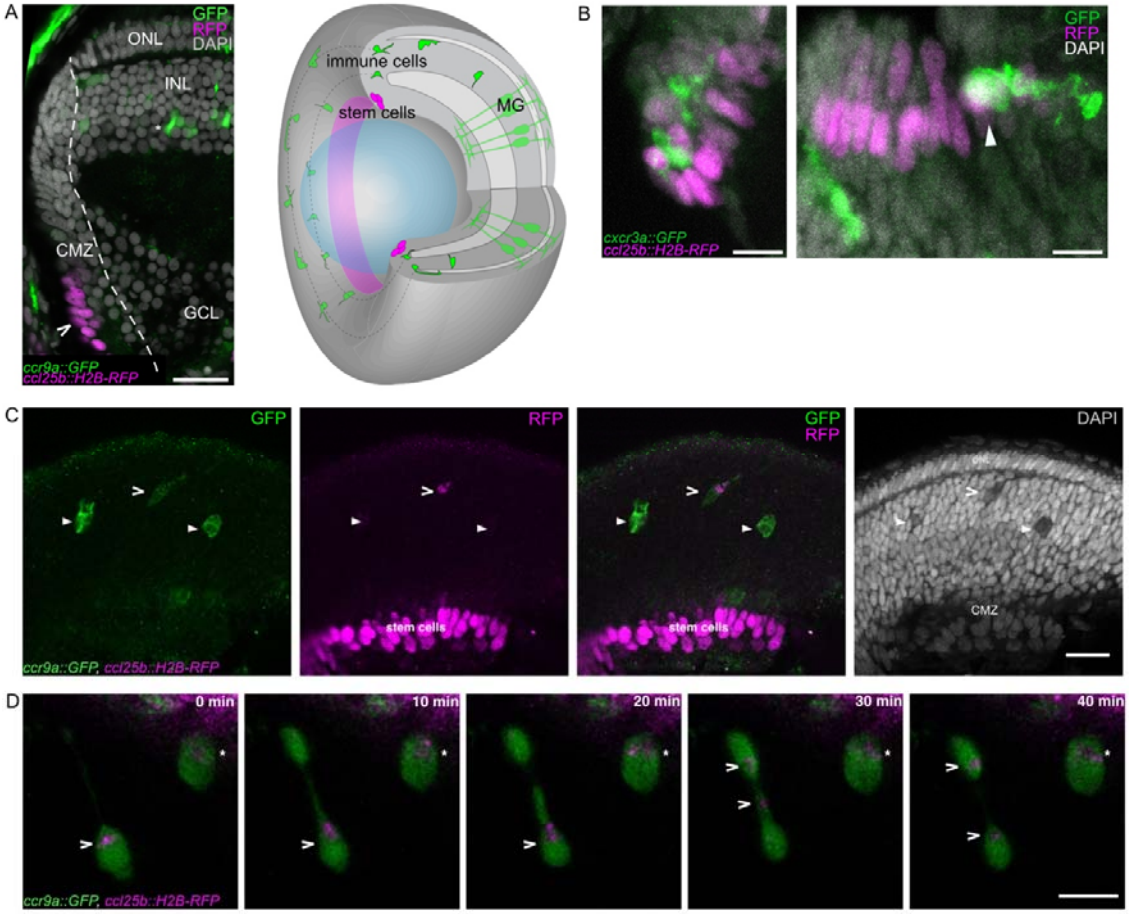

Figure 2: Ccl25b expressing RSC are phagocytosed by ccr9a+ microglia.

(A) Transverse section of a *ccl25b::H2B-RFP_ccr9a::GFP* reporter retina of a hatchling. *Ccl25b*-driven H2B-RFP expression (open arrowheads) is located in the peripheral CMZ (dashed line). *Ccr9a*-driven GFP expression can be detected in single cells of the dorsal CMZ as well as in MG cells in the differentiated part of the retina (asterisk). Scale bar: 20 µm. 3D schematic representation of a retina expressing illustrating the distribution of *ccl25b* expressing RSCs (magenta) and *ccr9a* expressing microglia cells (green). (B) Retinal stem cell region showing interaction between H2B-RFP expressing *ccl25b+* (magenta) and GFP expressing *cxcr3a* positive cells (green), detected by antibody staining against RFP and GFP in wholemount retinae. Arrowhead indicates phagocytic cup in the process of forming. Scale bar: 10 µm. (C) Wholemount staining showing the CMZ and retinal layers expressing H2B-RFP *in ccl25b* positive RSCs and GFP expressing in ccr9a+ microglia cells. White arrowheads depict *ccr9a* expressing cells enclosing H2B-RFP fractions (magenta) within phagosomes. Scale bar: 20 µm. (D) Time lapse of a *ccl25b::H2B-RFP* (magenta), *ccr9a::GFP* (green) retina depicting an immune cell transporting phagosomes within the

CMZ (open arrowheads) and a static immune cell with a phagosome (asterisk). Scale bar: 10 µm.

Activity of microglia is dependent on *ccl25b* chemokine

The RSC specific expression of the chemokine ligand *ccl25b*, combined with our finding of *ccr9a* positive immune cell-mediated stem cell phagocytosis, suggests that the ligand provides localized guidance cues that direct the pruning activity of *ccr9a*-positive immune cells.

To address the role of Ccl25b in the microglia mediated pruning of RSCs we generated a *ccl25b*$^{-/-}$ mutant allele by targeted mutagenesis using CRISPR/Cas9. This allowed to test if the absence of Ccl25b affects the interaction between RSCs and immune cells. Targeted mutagenesis was designed to delete the majority of the *ccl25b* gene and the mutant transcript contained only 22 % of the wild type coding sequence. The mutated gene was lacking the CC motif crucial for folding and function of CC class chemokines (Thomas et al., 2015) (Fig. 3 S1A).

The effect of loss of *ccl25b* functionality on phagocytosis, was assessed in *ccl25b*$^{-/-}$ mutants in the background of the *ccl25b::H2B-RFP*, *ccr9a::GFP* double reporter line. We examined the number of immune cells containing RSC-derived phagosomes in homeostatic conditions. We found that in wild type fish RSC-derived phagosomes were present in 61 % of *ccr9a*-positive cells (n = 201/331 cells in 8 retinae). In *ccl25b*$^{-/-}$ mutants the number of *ccr9a*-positive cells containing RSC-derived H2B-RFP-positive phagosomes was reduced to 36 % (Fig. 3A') (n = 113/317 cells in 6 retinae). Moreover, there was no significant change observed in the number of *ccr9a*-positive cells as well as the number of RSCs expressing *ccl25b::H2B-RFP* did not differ in the absence of the Ccl25b chemokine (Fig.3 S1B, Fig . 3B). The comparison of transverse sections of 3-week post hatch retinae between wildtype and *ccl25b-/-*, showed no gross morphological changes (Fig. 3 S1D-D').

Since chemokines are known to have a key function in acute injury responses, by attracting immune cells towards the site of inflammation(Sokol & Luster, 2015), we addressed whether Ccl25b is required to direct the migration of *ccr9a*-positive microglia within the retina to the stem cell domain upon injury. We used two-photon mediated RSC ablation to inflict a wound to the stem cell niche in the retina at hatching stage as has been described previously(Lust & Wittbrodt, 2018). We recorded the response of immune cells to the injury over four hours, with a temporal resolution of 2 min and analyzed their speed and directionality. In wild type retinae, *ccr9a*-positive cells migrated rapidly to the injured area (Fig. 3C-F) while in *ccl25b*$^{-/-}$ retinae, the migratory behavior of *ccr9a*-positive cells was significantly reduced and lacked directionality. In general, they displayed lower average migration velocity and travelled shorter total distances in the absence of Ccl25b (Fig. 3D-F).

These results indicate a crucial role of the Ccl25b-Ccr9a signalling axis in giving direction and specificity to microglia impacting on their ability to phagocytose stem cells without affecting the overall stem cell number.

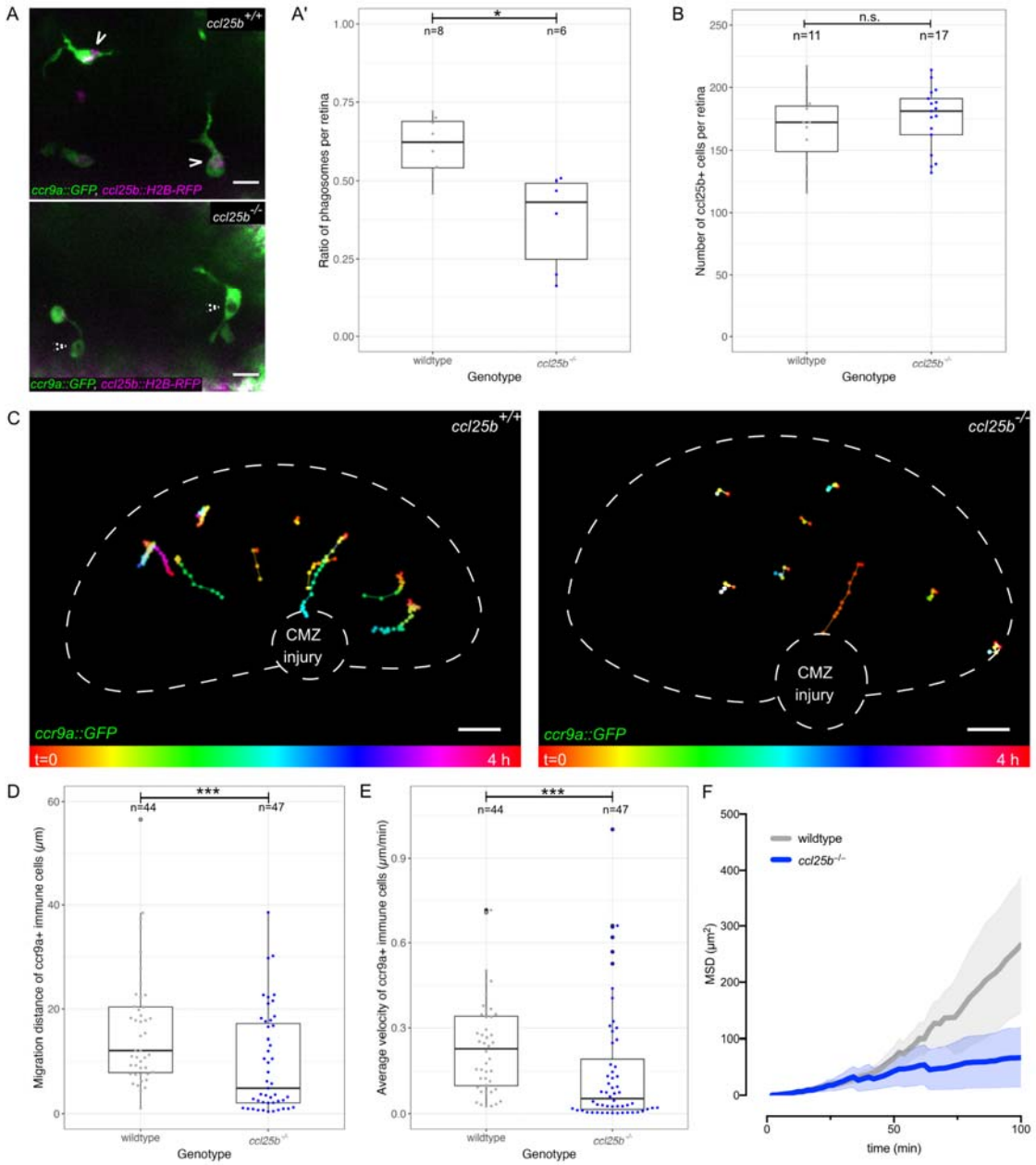

Figure 3: Ccl25b chemokine is necessary for activity of ccr9a positive immune cells in response to injury

(A) Representative images of phagosomes in wild type and *ccl25b*$^{-/-}$ retinae of *ccl25b:H2B-RFP* reporter fish. Scale bar: 10 µm. (A') Comparison of percentage of *ccr9a*-positive immune cells with H2B-RFP-positive phagosomes in wildtype (n = 8) and *ccl25b*$^{-/-}$ (n = 6)

retinae (*p = 0.01039; unpaired t-test). (B) Quantification of *ccl25b+* retinal stem cells in wildtype (n=11) and *ccl25b*$^{-/-}$ (n=17) (p=0.487; unpaired t-test). (C) Representative tracks with temporal color-coding representing immune cell migration in *ccr9a::GFP* hatchling retinae in WT (n = 44 cells from 5 fish) and *ccl25b*$^{-/-}$ (n= 47 cells from 7 fish). Scale bar: 20 µm. (D) Quantification of immune cell migration distance in the retinae of *ccl25b*$^{-/-}$ vs wild type hatchlings (***p = 0.0008512; Mann Whitney U test). (E) Quantification of average migration velocity of immune cells in the retinae of WT compared to *ccl25b*$^{-/-}$ hatchlings (***p = 0.0001817; Mann Whitney U test). (F) Analysis of mean square displacement (MSD) as a function of time from immune cell tracking data. MSD of *ccl25b*$^{-/-}$ compared to MSD of immune cells in WT retinae. Paler shading indicates standard error of means (SEM).

Absence of microglia affects the retinal stem cell numbers

Since we observed that phagocytosis is reduced but not inhibited in the absence of the Ccl25b chemokine, we investigated if the regulation of the RSC population is affected by the absence of microglia. Elimination of microglia was achieved by targeted inactivation of a transcription factor, *spi1b*, which is essential for the differentiation of cells of the lymphoid and myeloid lineages (Rhodes et al., 2005; Roh-Johnson et al., 2017; Scott et al., 1994).

Using CRISPR/Cas9-targeted mutagenesis, we generated a *spi1b*$^{-/-}$ mutant carrying a 6 bp insertion and 10 bp deletion in the 5th exon of *spi1b*, resulting in a premature stop codon (Fig. S3A-A') truncating the C-terminus of the Spi1b protein. This resulted in the absence of macrophages as validated by Sudan black staining and in situ hybridization using a *cxcr3a* probe. In *spi1b*$^{-/-}$ homozygous mutants, Sudan Black stained blue-black cells were absent from the tail fin (Fig. S3B-B') as were *cxcr3a* labelled macrophages in the brain, gills, intestine and skin of the hatchlings where they can usually be found in the wildtype (Fig. S3C-C'). The loss of *spi1b* is lethal at a juvenile stage (3 weeks post hatching).

To investigate whether retinal stem cells and the CMZ are affected in the absence of microglia, we established a *ccl25b::H2B-RFP* reporter line heterozygous for the *spi1b*$^{+/-}$ mutant allele. The *ccl25b::H2B-RFP* positive, *spi1b*$^{+/-}$ heterozygous mutant adults were in-crossed to obtain offspring that lack microglia. The absence of microglia in *spi1b*$^{-/-}$ hatchlings resulted in an expansion of the RSC population represented by an increased width of the RFP-positive RSC domain at the hatching stage (Fig4A-A'). Quantification across the entire CMZ showed a 34.3% increase in RSC numbers in the absence of microglia (*spi1b*$^{-/-}$: n = 13 retinae; wild-type siblings: n = 51 retinae) (Fig. 4B). This expansion of the *ccl25b* positive RSC pool in *spi1b*$^{-/-}$ mutants persists after hatching until mutant fish die at approximately 3 weeks post hatching. The increase in RSC numbers is presented here in an exemplary section of the CMZ in a young fish 5 days post hatching (Fig. 4C-C'). We also measured the retina size and length of these mutant hatchlings to observe differences at the physiological

level. As represented in Fig. 4D, the retina of the *spi1b-/-* hatchling are asymmetrical in their size and the length of the fish is slightly smaller. Quantification of the ratios of the left and right retina to their body length do not show any positional differences (Fig. S3D) but when the sizes are grouped into small and big retina across the genotypes, we observed that the retina of the spi1b-/- are significantly smaller compared to the wildtype and heterozygous mutants (Fig. 4D'). This indicates that the absence of microglia, affects the overall retinal tissue growth. Our data show that microglia regulate retinal stem cell numbers to maintain proper tissue architecture under homeostatic conditions.

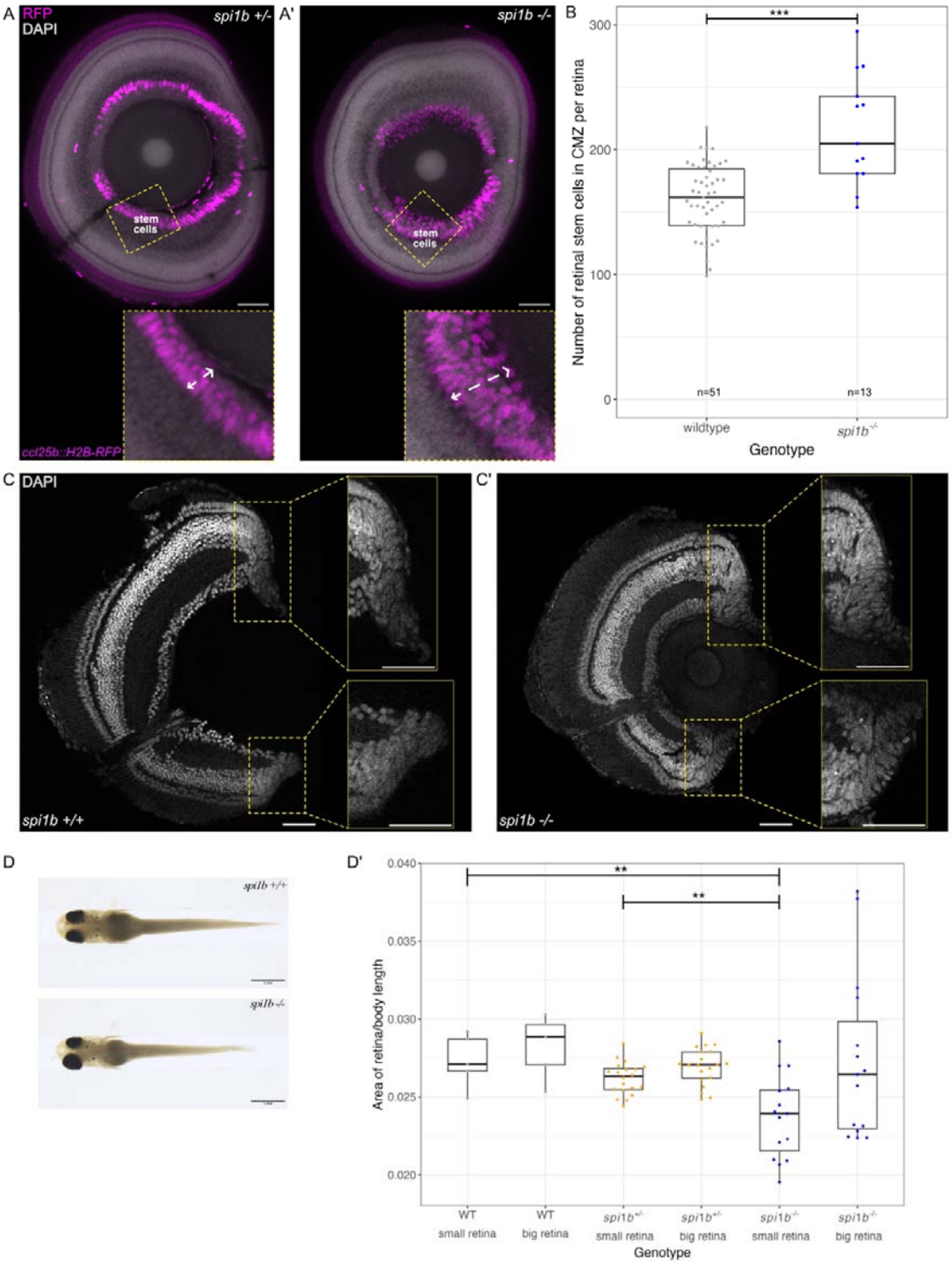

Figure 4: Ccl25b retinal stem cells are affected in absence of microglia

(A) Sagittal view on retinae of *ccl25b:H2B-RFP* reporter hatchlings with WT and *spi1b-/-* background. H2B-RFP was detected by antibody staining of whole retina (magenta) (zoomed in box shows width of the RFP positive cells). Scale bar: 50 µm. (B) Comparison of *ccl25b* expressing retinal stem cells in wildtype hatchings (n=26 fish) and *spi1b-/-* hatchlings

(n=7 fish) (***p = 0.0006511; unpaired t-test). (C-C') Transverse section of wildtype and *spi1b -/-* retina stained with DAPI (grey) at 5 days post hatch. CMZ region is highlighted and zoomed in (yellow box) showing nuclei organization. Scale bar: 50 µm. (D) Dorsal view of wildtype and *spi1b-/-* hatchlings to visualize differences in the size of retina. Scale bar is 1 mm. (D') Quantification of size of the retina by area normalized with the length of the fish to see any differences between wildtype (n=5), spi1b+/- (n=20) and spi1b-/- (n=15). The retina sizes are grouped into small and big retina for every hatchling. (p = 0.005261 for WT small retina vs. spi1b-/- small retina, p = 0.003576 for spi1b+/- small retina vs. spi1b-/- small retina; unpaired t-test).

Discussion

Our research reveals that microglia play a crucial regulatory role in controlling the numbers of retinal stem cells (RSC) in medaka. The life-long activity of the RSC niche, marked by *ccl25b* expression, requires extrinsic regulation by microglia in an apoptosis independent manner. The absence of microglia surveillance in *spi1b*$^{-/-}$ mutants, results in RSC expansion and consequently in an enlarged stem cell niche (CMZ).

While the Ccl25-Ccr9 signalling pathway had previously been associated with antigen presentation in the intestine and T cell development in the thymus (Aghaallaei et al., 2022; Baubak Bajoghli, 2009), our observations demonstrate an additional function. We show that microglia, an innate immune cell that has not been previously linked to this pathway, express the *ccr9a* receptor and is involved in direct stem cell interaction. This highlights the tissue-specific role of Ccl25-Ccr9 signalling and its ability to influence both myeloid and lymphoid cell types differently.

Loss of Ccl25b specifically impairs microglial migration towards the site of injury in the CMZ and disrupts homeostatic phagocytosis of retinal stem cells. Although chemokines are known to facilitate immune cell homing during development (Wurbel et al., 2007; Wurbel et al., 2001), the absence of *ccl25b* in mutant retinae did not affect the presence of *ccr9a* microglia at the interface between CMZ and central retina, indicating that Ccl25b is dispensable for microglia residence in retinal tissue. While microglia actively express the *ccl25b* receptor *ccr9a*, and an inflammatory response after injury is clearly affected without Ccl25b, this pathway is not essential for regulating stem cell numbers. This argues for an alternative mechanism of stem cell-microglia interaction, a form of "homeostatic stem cell pruning".

While the knowledge about interaction between immune and stem cells has been rather limited, a similar regulatory mechanism by immune cells has recently been described for the hematopoietic stem cell niche (HSC) in zebrafish (Wattrus et al., 2022). The underlying

mechanisms functioning in neuronal stem cells and microglia interaction in the medaka retina remain to be explored.

The teleost retina exhibits continuous, highly organized growth dependent on tightly regulated stem cell activity, and we demonstrate that microglia maintain this balance by phagocytosing RSCs. A fundamental question is whether this regulation serves as a quality control mechanism where specific cells display markers targeting them for phagocytosis, or if the process is stochastic, based on physical constraints within the CMZ similar to other developmental processes where cell elimination occurs through mechanical or signaling mechanisms(Huels et al., 2018; Levayer et al., 2016). This newly discovered role of the immune system opens exciting possibilities for understanding its involvement in the transition to and maintenance of multicellularity during development, providing an excellent foundation for exploring key mechanisms in stem cell niche regulation.

Materials and Methods:

Fish husbandry and transgenic lines

Medaka (*Oryzias latipes*) were kept as closed stocks at Heidelberg University. All experimental procedures and husbandry were performed in accordance with the German animal welfare law and approved by the local government (Tierschutzgesetz §11, Abs. 1, Nr. 1, husbandry permit AZ 35–9185.64/BH and line generation permit AZ 35–9185.81/G-145-15). Fish were maintained in a constant recirculating system at 28°C on a 14 h light/10 h dark cycle. The following previously described stocks and transgenic lines were used for this study: wild-type Cab, *rx2::H2B-RFP(Reinhardt et al., 2015), ccr9a::GFP(Bajoghli et al., 2015), ccl25b::GFP, ccr9a:mCherry, ccl25b::H2B-RFP(Aghaallaei et al., 2022)*, GaudíRSG (Centanin et al., 2014) and cxcr3a::GFP (Aghaallaei et al., 2010).

The following lines were generated for this study: *ccl25b*$^{-/-}$, *ccl25b::Cre*^{ERT2}, *spi1b*$^{-/-}$. Transgenic lines were created by microinjection with Meganuclease (I-SceI) in medaka embryos at the one-cell stage, as previously described(Thermes et al., 2002).

CRISPR/Cas9 mediated mutation of the ccl25b and spi1b locus

For generating truncated variants of *ccl25b* and *spi1b* we used CRISPR/Cas9 mediated mutation. The medaka *ccl25b* gene (GENE ID: ENSORLG00000028881, Exon ID: ENSORLE00000270681) comprises six exons. We selected two sgRNAs targeting the CC motif in Exon 4. The following target sites were used (PAM in brackets): GCGCCAATCCAGAGGACCCG(TGG) and CTTGGCTACGTGAGAGAACT(CGG). For

mutation of Spi1b we used one sgRNA targeting exon 5 of the *spi1b* gene: GAGGCCCTCGCACACCGCTGGG (Gene ID: ENSORLG00000006090, Exon ID: ENSORLE00000068479. All sgRNAs were designed using the CCTop prediction tool (Stemmer et al., 2015). Cloning of sgRNA templates and in vitro transcription was performed as described previously. The pCS2+Cas9 plasmid was linearized using NotI and the mRNA was transcribed *in vitro* using the mMessage mMachine SP6 kit (ThermoFisher Scientific, AM1340). The CRISPR generated edits were mapped and analysed using geneious software version 2019.2.3 (www.geneious.com).

One-cell stage medaka were injected with 150 ng/µl of Cas9 mRNA and 15 ng/µl of the sgRNAs. Injected embryos were maintained at 28°C in embryo rearing medium (ERM, 17 mM NaCl, 40 mM KCl, 0.27 mM $CaCl_2$, 0.66 mM $MgSO_4$, 17 mM Hepes). One day post injection (dpi) embryos were screened for survival.

Genotyping and mutant selection

For genotyping either injected F0 embryos or fin clips of juvenile or adult fish were lysed in DNA extraction buffer (0.4 M Tris/HCl pH 8.0, 0.15 M NaCl, 0.1 % SDS, 5 mM EDTA pH 8.0, 1 mg/ml proteinase K) at 60°C overnight. Proteinase K was inactivated at 95°C for 10 min and the solution was diluted 1:2 with H_2O.

The PCR amplification was performed with Q5 polymerase (NEB) according to the manufacturers protocol using 30 PCR cycles. The resulting PCR product was analysed on a 1% agarose gel. F0 animals were raised to adulthood and outcrossed to wild type Cab fish. F1 fish were then raised to adulthood and finclipped and genotyped. Mutants carrying the same allele were incrossed to obtain homozygous mutants.

To identify mutations in the locus, fin clip DNA of F1 fish was analysed as described above. Genotyping of ccl25b mutants revealed a 333 bp deletion in the ccl25b locus, completely eliminating exon four including the CC motif along with two-thirds of exon five (Figure 3 Supplement 1). Transcript analysis of wild type and *ccl25b*$^{-/-}$ fish showed that the resulting truncated transcript contained only 22% of the wild type coding sequence. We selected *spi1b*$^{-/-}$ mutants carry a 6bp insertion and 10bp deletion in exon 5 which leads to a frame shift and premature stop codon.

Tamoxifen induction of Cre/lox recombination in ccl25b expressing cells

For Cre^{ERT2} induced recombination of *ccl25b* expressing cells, *ccl25b::Cre*^{ERT} X *GaudiRSG* (Centanin et al., 2014) hatchlings (0 day post hatch) were treated with 5 µM tamoxifen solution (Sigma-Aldrich) in 1x ERM overnight. Fish were then grown for 3 days or six weeks before they were sacrificed for whole mount immunostaining of retinae as described below.

Immunohistochemistry on whole-mount retinae

ccl25b::CreERT X GaudiRSG fish grown for 6 weeks after induction of recombination were euthanized with 20x Tricaine (Stock: 4 g/l triciane; 10g/l Na2HPO4·2 H2O; pH 7-7.5), fixed overnight in 4 % PFA and treated and stained as described in(Perez Saturnino et al., 2018).

To detect GFP after Cre-induced recombination in *ccl25b* expressing cells we used chicken anti-eGFP (1:500, Life Technologies, A10262) and donkey anti-chicken Alexa Flour 488 (1:750, Jackson, 703-485-155) and DAPI (2 mg/ml) (1:500). Retinae of *cxcr3a::GFP;ccl25b::H2B-RFP* reporter hatchlings were treated and stained as in (Perez Saturnino et al., 2018) except bleaching time was reduced to 1h.

For the detection of GFP, we used chicken anti-eGFP (1:500, Life Technologies, A10262) and donkey anti-chicken Alexa Flour 488 (1:750, Jackson, 703-485-155). For detection of RFP, we used rabbit anti-RFP (1:500, Clontech 632496) as primary antibody and goat anti-rabbit DyLight549 (1:750, Jackson, 112-505-144) or goat anti-rabbit Alexa Fluor 647 (1:250, Thermo LifeTech, A21245) as secondary antibody. To visualize nuclei organization, retinae of *spi1b+/-* and *spi1b -/-* hatchlings were stained for DAPI (1:500) at 5 days post hatch.

BrdU incorporation assay

To follow cell division in *ccl25b* positive cells we incubated *ccl25b::GFP* reporter hatchling in 2.5 mM BrdU diluted in 1x Embryo Rearing Medium (ERM) for 1 day at 28°C. After removal of BrdU fish were euthanized, fixed and treated for cryo-sectioning.

Immunohistochemistry on cryosections

To obtain cellular resolution of the CMZ and surrounding cell layers, immunohistochemistry was performed on hatchlings as described previously(Lust & Wittbrodt, 2018). For the detection of GFP in *ccr9a:GFP* we used chicken anti-eGFP (Life Technologies, A10262) and donkey anti-chicken Alexa Flour 488 (Jackson, 703-485-155). For the detection of BrdU cryosections were fixed in 4% PFA (paraformaldehyde; pH 7) for 30 mins after the incubation with secondary antibody and DAPI. After fixation sections were washed 3x for 10 mins with 1x PTW. The sections were then treated with 2N HCl, 0.5% Triton X in 1x PBS for 60 min at 37°C for antigen retrieval, washed again 3x for 10 mins with 1x PTW and then treated with Borax/PTW for 15 mins for pH recovery. After washing 3x for 10 mins sections were blocked with 10% NGS in 1x PTW for 2 hours, then washed 2x for 5 mins with 1x PTW before applying the primary antibody (1:100 or 1:200 BrdU (Abcam, ab6326)) in 1% NGS) overnight at 4°C. The next day the sections were washed 6x for 10 mins with 1x PTW before secondary antibody was applied (1:750 anti-rat DyLight488 (Jackson, 112-485-143) in 1% NGS) for 2 hours at 37°C and sections were washed again with 1x PTW before mounting as described in(Lust & Wittbrodt, 2018).

In situ hybridization chain reaction (HCR)

HCR probe sets for *ccl25b*, *rx2* and *ccr9a* were designed against unique mRNA sequences, based on the Japanese medaka HdrR ASM223467v1 transcriptome. Probes (50pmol) were ordered as IDT Oligo pools. Alexa-488 and Alexa-594 conjugated hairpins were purchased from Molecular instruments together with the buffers. CUBIC-based clearing method was used to improve probe penetration (Susaki & Ueda, 2016 and http://www.cubic.riken.jp). Fixed and washed medaka hatchlings were incubated in 50% CUBIC-L/R1a (mixed 1:1 and then diluted to 50% in dH2O) for 30 mins at room temperature while shaking and moved to a 100% CUBIC-L/R1a solution for another 30 min incubation at room temperature on a shaker. Afterwards the embryos were washed 4 times 15 minutes with 1x PBS. HCR was performed according to the Molecular Instruments instructions. Probe concentration was increased to 4 pmol. Embryos were incubated with DAPI (1:500 in 5X SSCT) for 10 minutes at room temperature, transferred to a MatTek glass-bottom dish and equilibrated in CUBIC refractive index matching solution CUBIC R+(N) until transparent.

Imaging was performed using the 63x objective on Leica SP8 confocal microscope. Image processing was done using Fiji. Bright outliers (of 1 pixel radius) were removed to denoise the image. Plugin “Subtract background” was used to correct background (rolling ball diameter = 75 pixels). Maximum projection of 6-10 z-slices (1µm z-step).

TUNEL staining

To measure the amount of apoptotic cells, we made use of In situ cell death detection kit,TMR red (Roche, 12156792910). To stain cryosections, 50 µl TUNEL reaction mix was added per slide and incubated at 37°C for 1 hr. Slides were washed twice with 1X PTW and mounted in 60% glycerol. For whole mount staining, retinae was permeabilized using 0.1% Triton X-100, 0.1% sodium citrate for 30 min at RT. Samples were washed twice with 1X PTW and incubated with the TUNEL reaction mix at 37°C for 1 hr in the dark. After washing twice with 1X PTW, they were mounted for imaging.

In vivo imaging and laser induced injury

For in vivo imaging, transgenic Cab embryos were kept in 5x 1-phenyl-2-thiourea (PTU (0.0165% m/v), Sigma) in 1x ERM from 1 dpf until imaging to block pigmentation. For embryonic stage imaging, stage 34 embryos were hatched using labmade hatching enzyme. Live hatchlings were anaesthetized in 1x Tricaine diluted in 1x ERM and mounted in glass bottomed Petri dishes (MaTek) in 1 % low melting point agarose.

In vivo imaging and laser ablations were performed on a Leica TCS SP8 and SP5 microscope equipped with a Spectra Physics Mai Tai® HP DeepSee Ti:Sapphire laser,

which has a tuneable wavelength range from 690-1040 nm, and Leica Hybrid Detectors. The retinal injury was induced using a 14x zoom in combination with the high-energy 2-photon laser, precisely tuned to 880 nm. Subsequent follow-up imaging for GFP detection was conducted using the identical laser wavelength of 880 nm and a 40x long distance objective. Imaging of double reporter fish was performed on a Leica DIVE microscope.

Sudan black staining

For visualising macrophages in medaka hatchlings we used Sudan black staining as described in(Aghaallaei et al., 2022). Medaka embryos were fixed in 4% PFA overnight, washed with PTW and incubated in Sudan black staining reagent (Sigma Aldrich 380B-1KT) for 1 hour in the dark. After staining, embryos were washed 3x with 70% EtOH and 3x with PTW. Pigments were bleached using 3% H2O2 + 0.5 % KOH for 15 min and embryos were washed again 3x with PTW before they were counterstained with Hematoxylin staining solution for 1 hour. Whole hatchling stained with Sudan black were captured using a Nikon SMZ18 Stereomicroscope fitted with a Nikon DS-Ri1 camera.

In situ hybridization

For visualising macrophages in medaka hatchlings whole mount *in situ* hybridization was performed using digoxygenin labelled *cxcr3a* probe transcribed from the cDNA of the second exon of the gene (ENSORLG00000013459.2). Medaka hatchlings from *spi1b* mutant line were fixed in 4% PFA overnight, washed with PTW and permeabilized with Proteinase K for 10 min. Whole mount *in situ* hybridization using NBT/BCIP solution was carried out as described previously (Loosli et al., 1998). After staining, hatchlings were washed 3x with PTW and mounted on microscopic slides with 60% glycerol in PBS. Images were acquired using Nikon Eclipse 80i microscope.

Immunohistochemistry imaging

All cryosections and whole mount samples were imaged using an inverted confocal laser scanning microscope Leica TCS SP8. The microscope was equipped with ACS APO objective lenses (10x/0.3 dry, 20x/0.75 multi-immersion, 63x/1.3 glycerol) and featured laser lines at 405 nm, 488 nm, 532 nm, and 638 nm. The system was configured with two PMT detectors. For whole mount sample imaging, retinae were mounted in MatTek dishes using 1% low melting agarose in 1x PTW or clearing solution ((Zhu et al., 2019)(20% (wt/vol) urea (Sigma–Aldrich, Cat#: V900119), 30% (wt/vol) D-sorbitol (Sigma–Aldrich, Cat#: V900390), 5% (wt/vol) glycerol (Sigma–Aldrich, Cat#: V900122) dissolved in DMSO (Sigma Aldrich, Cat#: V900090))., with the Ciliary Marginal Zone (CMZ) positioned touching the bottom of

the dish. After the agarose solidified, the dish was covered with 1x PTW. No solution was added on top in case of clearing solution.

Image acquisition of hatchlings

To measure the size of the retina and length of the *spi1b* wildtype and mutant hatchlings, samples were fixed in 4% PFA in PTW and mounted in 1.5% agarose plates with customized wells. Images were acquired using Nikon SMZ18 microscope with DS-Ri1 camera.

Image processing and statistical analysis

Images were processed using the Fiji image processing software. Statistical analysis and graphical representation of the data were performed using RStudio and Prism software package (GraphPad)(*RStudio: Integrated Development Environment for R.*, 2023). Tracking of immune cells was carried out using MTrackJ plugin in Fiji. Average velocity, migration distance and mean square displacement (MSD) as a function of time were calculated for each immune cell. Average velocity over time and total migration distance were calculated for each individual immune cell. The MSD at time point t was calculated as the squared distance between immune cell position at time point t and at t = 0. Box plots show median, 25th and 75th percentiles. Cell counting was done using cell counter plugin in Fiji. Unpaired t-tests and Mann Whitney test were performed to determine the statistical significances. The P value $P < 0.05$ was considered significant and P values are given in the figure legends. Sample size (n) is mentioned in figure legends. The experimental groups were allocated randomly, and no blinding was done during allocation. The figures in this study were created using the software Affinity Designer 2, version 2.5.5 (2024), Serif.

Acknowledgments:

We thank the Wittbrodt lab for constructive discussions on the project, Lazaro Centanin, Carmen Gloria Feijoo, Tinatini Tavhelidse-Suck, Thomas Thumberger, Erika Tsingos and Lucie Zilova for critical reading of the manuscript. We are grateful to Leica Microsystems Germany, in particular K.-H. Körtje for providing access to and assistance with the Leica DIVE imaging setup. We are grateful to Tanja Kellner and Beate Wittbrodt for expert technical assistance. Pimpan Sujariyakul for work on establishing the *spi1b* mutant line and Nithyapriya Kumar for studying the embryonic and post-embryonic phagocytosis behavior. We thank Erik Leist and Marzena Majewski and Antonino Saraceno for fish husbandry. K.L., C.B. and R.A. were members of HBIGS, the Heidelberg Graduate School for Life Sciences. K.L. was supported by a LGFG Fellowship by the Ministerium fu□r Wissenschaft, Forschung und Kunst Baden-Wu□rttemberg. C.B. was supported by a PhD fellowship of the

Studienstiftung des deutschen Volkes. O.S. was supported by an HBIGS MSc fellowship. This work was supported by the European Research Council (GA 294354-ManISteC and synergy grant 810172/IndiGene to J.W.), the BMBF-grant "KI-Morph" (to J.W., 05023VH2) and the Deutsche Forschungsgemeinschaft (SFB 873 TP A3 to J.W.).

Author contributions

R.A., K.L., C.B., J.B and J.W. conceived the study and designed the experiments and J.W. supervised the work. R.A., K.L., C.B., J.B., N.F., F.E. and O.S. performed, discussed and refined the experiments in constant discussion with J.W.. B.B. and N.A. contributed transgenic fish lines and conceptual input. R.A., K.L., C.B., J.B., E.HdC. and J.W. wrote the manuscript with feedback from all authors.

Competing interests: Authors declare no competing interests.

Data and materials availability: All data are available in the main text or the supplementary materials.

Supplementary Materials:

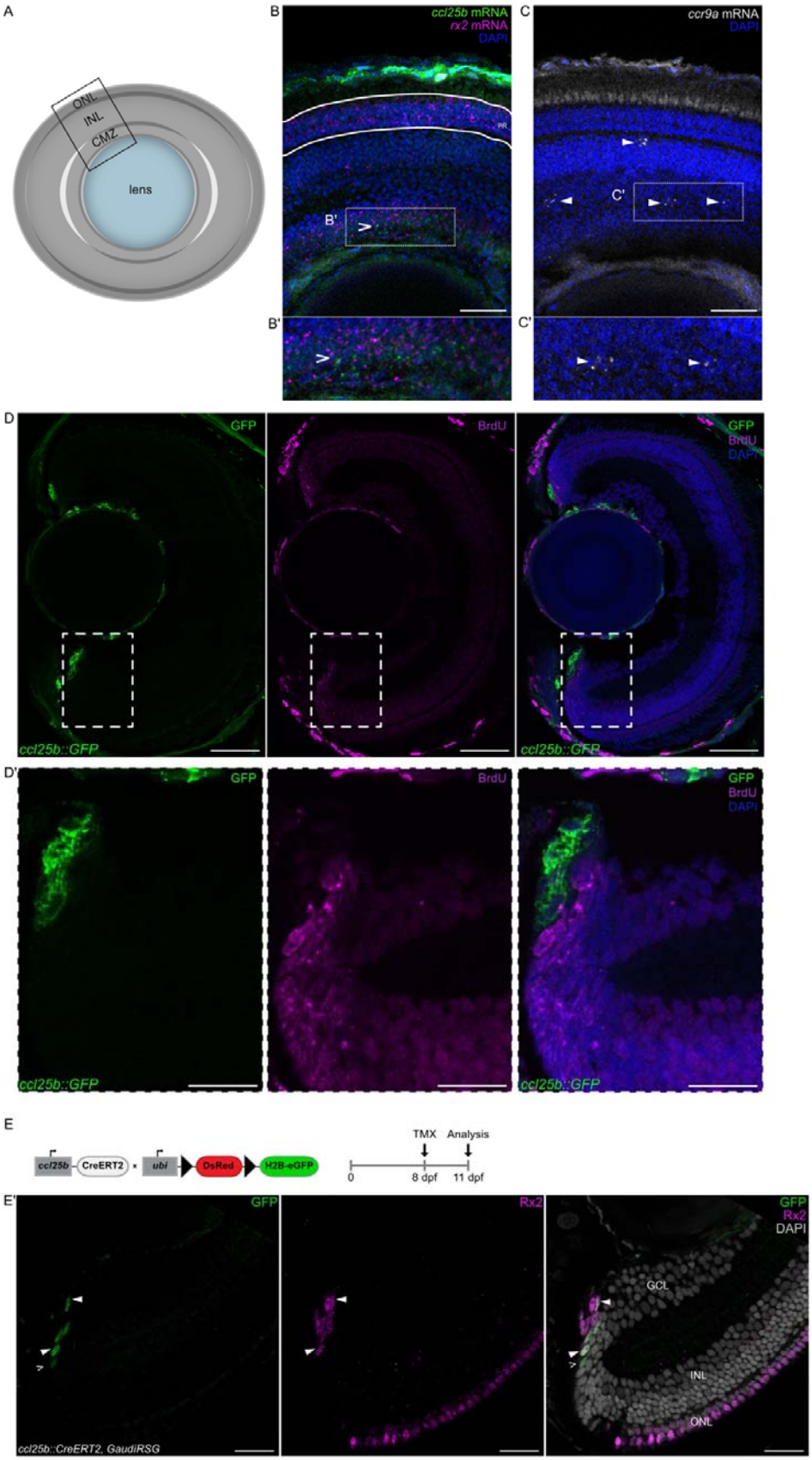
A
ONL
INL
CMZ
lens
B
ccl25b mRNA
rx2 mRNA
DAPI
PR
B'
C
ccr9a mRNA
DAPI
C'
B'
C'
D
GFP
BrdU
GFP
BrdU
DAPI
ccl25b::GFP
ccl25b::GFP
D'
GFP
BrdU
GFP
BrdU
DAPI
ccl25b::GFP
ccl25b::GFP
E
ccl25b
CreERT2
ubi
DsRed
H2B-eGFP
TMX
Analysis
0
8 dpf
11 dpf
E'
GFP
Rx2
GFP
Rx2
DAPI
GCL
INL
ONL
ccl25b::CreERT2, GaudiRSG

598

Figure 1 Supplement 1: ccl25b and ccr9a endogenous expression in the retina and proliferative behaviour of ccl25b+ cells

(A) Schematic diagram of a whole retina showing the different regions: the CMZ (stem and progenitor cell region) and inner and outer nuclear layers (INL and ONL) (differentiated regions). Box shows the area of the retina represented in B and C. (B) Hybridisation chain reaction (HCR) *in situ* staining of *ccl25b* and *rx2* mRNA to detect their endogenous expression in differentiated retinal layers and the CMZ region (B'). Scale bar: 20 µm. (C) HCR *in situ* staining of *ccr9a* mRNA in the retinal layers and specifically in the INL (white box, C'). Scale bar: 20µm. (D) Transverse section of a *ccl25b::GFP* hatchling retina stained for BrdU incorporation after a short 24 h BrdU pulse. BrdU positive cells in relation to *ccl25b* expressing RSC at the periphery of CMZ. Scale bar: 50 µm. (D') Marked area of CMZ as shown in D (white box). Scale bar: 20 µm. (E-E') Earliest induction of *ccl25b::Cre* expressing cells (3 days post induction). Recombined cells express GFP and co-localise with rx2 positive cells (white filled arrows) at the beginning and eventually do not co-localise with rx2 (white line arrow) as the recombined stripe grows. Scale bar: 20µm.

Figure 2 Supplementary movie 1: Distribution of microglia throughout the retina. Microglia expressing *cxcr3a::GFP* are visualized using immunostaining in a post-embryonic whole mount retina (0 days post hatch). They are mainly positioned at the proximal edge of the CMZ near inner plexiform layer (IPL) and outer plexiform layer (OPL) as two concentric rings. In addition, they are also seen in other regions since they are migratory cells. White circle: lens, yellow circle: first ring of microglia near IPL, magenta circle: second ring of microglia near OPL. Scale bar is 50µm.

Figure 2 Supplementary movie 2: *Ccr9a*-positive immune cells with H2B-RFP positive phagosomes derived from ccl25b expressing cells.

In vivo imaging of a *ccl25b::H2B-RFP* (magenta), *ccr9a::GFP* (green) retina depicting mobile and static microglia containing H2B-RFP positive phagosomes within the CMZ and a static immune cell with a phagosome. Scale bar: 10 µm.

Figure 2 Supplementary movie 3: Microglia interacts with retinal stem cells expressing *ccl25b::h2BRFP*. In vivo imaging of an embryonic stage retina where microglia labelled with *cxcr3a::GFP* (green) interacts with *ccl25b* expressing retinal stem cells (magenta) by migrating in and out of the CMZ (interaction point at 01h 02min). Time interval is every 5 min 24 sec. Scale bar is 20 µm.

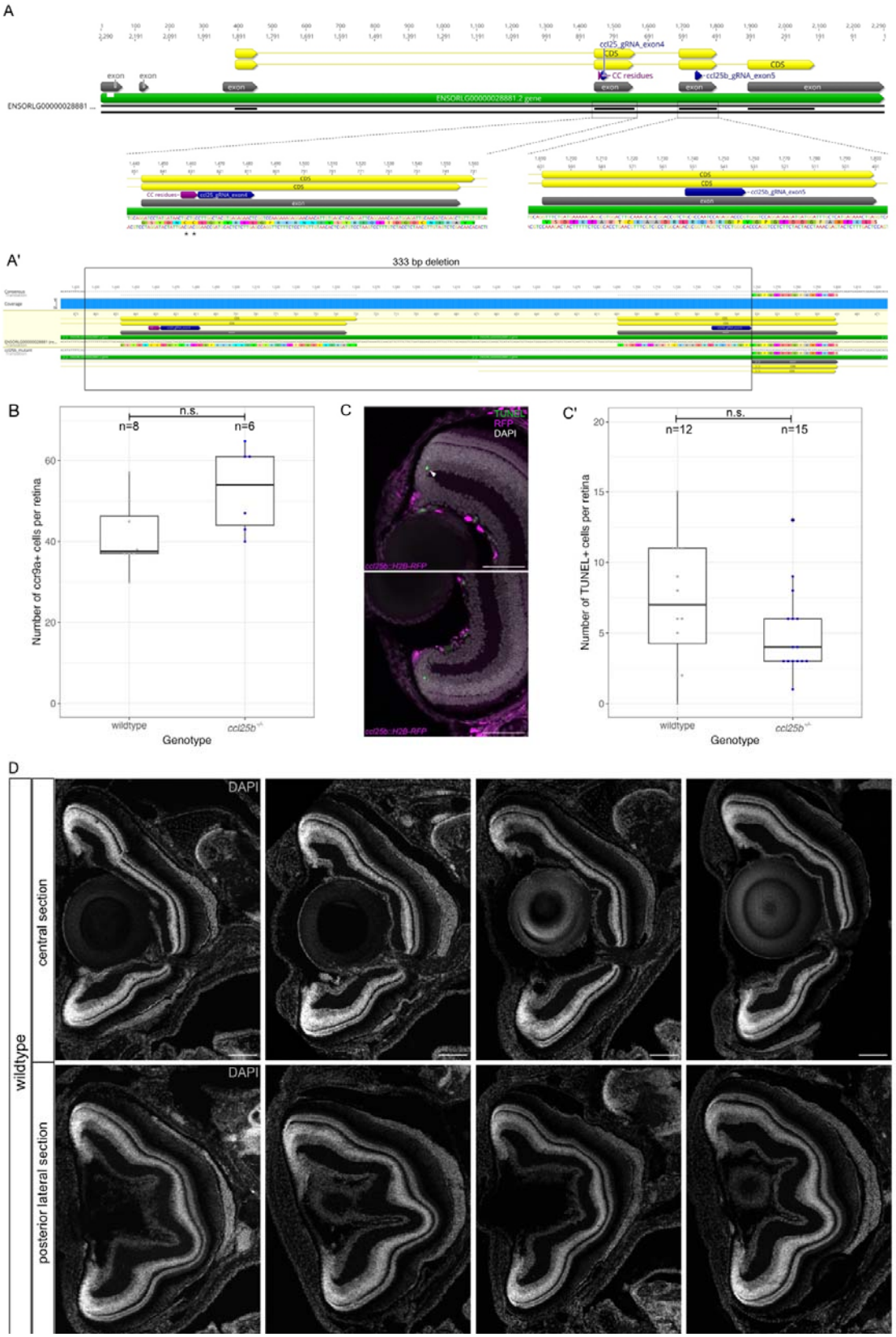
A
ccl25_gRNA_exon4
CDS
CC residues
ccl25b_gRNA_exon5
exon
ENSORLG00000028881.2 gene
A'
333 bp deletion
B
n.s.
n=8
n=6
Number of ccr9a+ cells per retina
wildtype
ccl25b-/-
Genotype
C
TUNEL
RFP
DAPI
ccl25b:H2B-RFP
C'
n=12
n=15
Number of TUNEL+ cells per retina
D
DAPI
wildtype
central section
posterior lateral section

636

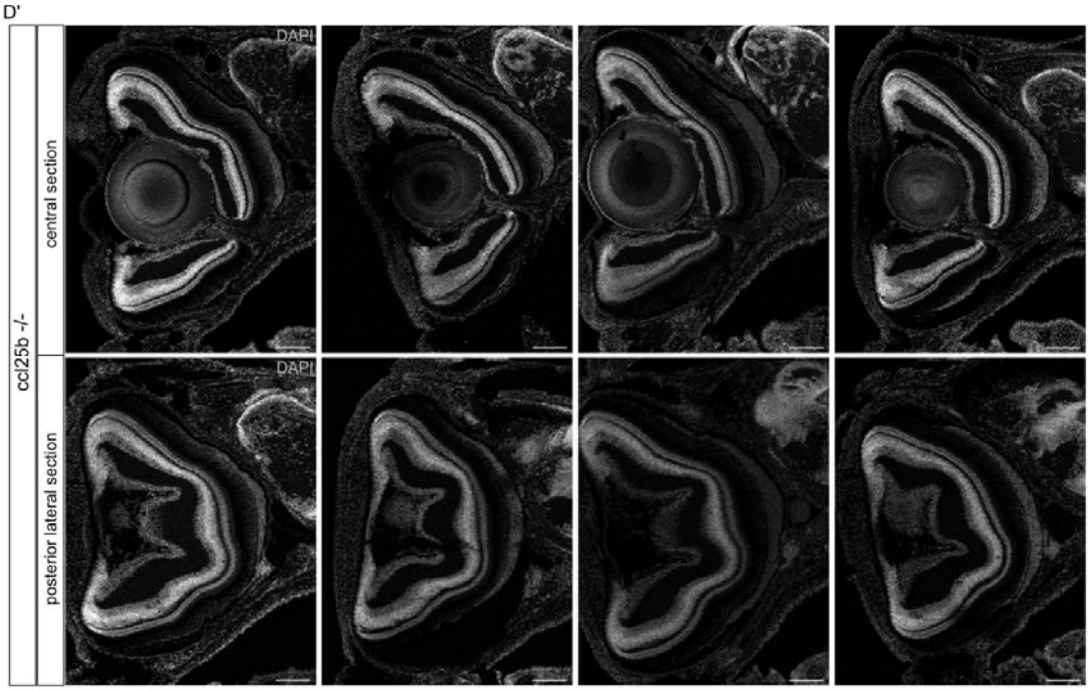

Figure 3 Supplement 1: Characteristics of *ccl25b* mutant

(A) Genomic locus of the *ccl25b* gene consisting of 6 exons, including the CC motif in exon 4 and the gRNA target sites in exon 4 and 5 (zoomed regions). (A') Sequence alignment of the ccl25b locus comparing wildtype and ccl25b−/− mutant fish. The alignment reveals a 333 bp deletion in the mutant that eliminates exon 4 (containing the CC motif) and a portion of exon 5. (CC motif: magenta, coding sequence (CDS): yellow, exon: grey, gene locus: green, sgRNA: blue) (B) Quantification of ccr9a+ cells in retinae of *ccl25b-/-* (n=6) compared to wildtype (n=8) (p = 0.05955; unpaired t-test). (C) Apoptotic cells (green) detected in a transversal section of a *ccl25b::H2B-RFP* reporter hatchling retina by TUNEL staining. Scale bar: 50 µm. (C') Quantification of apoptotic cells in wildtype (n=12) and *ccl25b-/-* (n=15) retinae using TUNEL assay. (p = 0.171; unpaired t-test). (D-D') Overall morphology observed in transverse sections of central and posterior region wildtype and *ccl25b-/-* retinae stained with DAPI. Scale bar: 100 µm.

A
spi1b_exon5_gRNA
spi1b- 101167188
spi1 gene
mRNA
CDS
A'
10bp deletion
6bp insertion
Consensus
Translation
Coverage
spi1b_wildtype
spi1b_mutant
premature stopcodon
B
spi1b+/+
B'
spi1b-/-
C
spi1b+/+
head (dorsal view)
gills and intestine (lateral view)
skin (lateral view)
C'
spi1b-/-
head (dorsal view)
gills (lateral view)
skin (lateral view)
D
Area of retina/body length
WT left retina
WT right retina
spi1b+/- left retina
spi1b+/- right retina
spi1b-/- left retina
spi1b-/- right retina
Genotype
D'
Length of fish (mm)
WT
spi1b+/-
spi1b-/-
Genotype

652

Figure 4 Supplement 1: The *spi1b* mutant lacks macrophages.

(A) Overview of genomic locus of the spi1b gene showing location of 5 exons and the gRNA target site in exon 5 (green:gene; red:mRNA ; yellow:CDS). (A') Genetic alignment of the mutated region in the spi1b site with the WT sequence demonstrating a 10 bp deletion and 6bp insertion which leads to a frameshift and hence a premature stop codon (black box with asterisk) in the *spi1b* mutant. (sgRNA: blue, mRNA:red). (B) Sudan black staining to visualize macrophages (white arrows) in WT and *Spi1b-/-* hatchling tails. Macrophages in the tail regions (white arrows) are absent in *spi1b-/-* fish. (C-C') In-situ hybridization of *cxcr3a* probe to visualize macrophages (black arrows and dotted line) in WT and *spi1b-/-* hatchling head, gill, intestine and skin of the posterior body. Macrophages are absent in *spi1b-/-* fish. (D) Ratio of left and right retina of WT (n=5), spi1b+/- (n=20) and spi1b-/- (n=15) hatchlings shows no significant difference in the eye sizes. (D') Length of WT (n=5), spi1b+/- (n=20) and spi1b-/- (n=15) hatchlings. (p = 0.009487 for WT vs. spi1b-/-, p = 7.403e-08 for spi1b+/- vs. spi1b-/-, p = 0.9391 for WT vs. spi1b+/- ; unpaired t-test).

References

Aghaallaei, N., Agarwal, R., Benjaminsen, J., Lust, K., Bajoghli, B., Wittbrodt, J., & Feijoo, C. G. (2022). Antigen-Presenting Cells and T Cells Interact in a Specific Area of the Intestinal Mucosa Defined by the Ccl25-Ccr9 Axis in Medaka. *Front Immunol*, *13*, 812899. https://doi.org/10.3389/fimmu.2022.812899

Aghaallaei, N., Bajoghli, B., Schwarz, H., Schorpp, M., & Boehm, T. (2010). Characterization of mononuclear phagocytic cells in medaka fish transgenic for a cxcr3a:gfp reporter. *Proc Natl Acad Sci U S A*, *107*(42), 18079-18084. https://doi.org/10.1073/pnas.1000467107

Arandjelovic, S., & Ravichandran, K. S. (2015). Phagocytosis of apoptotic cells in homeostasis. *Nat Immunol*, *16*(9), 907-917. https://doi.org/10.1038/ni.3253

Bajoghli, B. (2013). Evolution and function of chemokine receptors in the immune system of lower vertebrates. *Eur J Immunol*, *43*(7), 1686-1692. https://doi.org/10.1002/eji.201343557

Bajoghli, B., Kuri, P., Inoue, D., Aghaallaei, N., Hanelt, M., Thumberger, T., Rauzi, M., Wittbrodt, J., & Leptin, M. (2015). Noninvasive In Toto Imaging of the Thymus Reveals Heterogeneous Migratory Behavior of Developing T Cells. *J Immunol*, *195*(5), 2177-2186. https://doi.org/10.4049/jimmunol.1500361

Baubak Bajoghli, N. A., Isabell Hess, Immanuel Rode, Nikolai Netuschil, Boon-Hui Tay, Byrappa Venkatesh, Jr-Kai Yu, Stacy L. Kaltenbach, Nicholas D. Holland, Dagmar Diekhoff, Christiane Happe, Michael Schorpp, Thomas Boehm. (2009). Evolution of Genetic Networks Underlying the Emergence of Thymopoiesis in Vertebrates. *Cell*, *138*(1), 186-197. https://doi.org/https://doi.org/10.1016/j.cell.2009.04.017

Campbell, D. J., & Butcher, E. C. (2002). Intestinal attraction: CCL25 functions in effector lymphocyte recruitment to the small intestine. *J Clin Invest*, *110*(8), 1079-1081. https://doi.org/10.1172/JCI16946

Centanin, L., Ander, J. J., Hoeckendorf, B., Lust, K., Kellner, T., Kraemer, I., Urbany, C., Hasel, E., Harris, W. A., Simons, B. D., & Wittbrodt, J. (2014). Exclusive multipotency and preferential asymmetric divisions in post-embryonic neural stem cells of the fish retina. *Development*, *141*(18), 3472-3482. https://doi.org/10.1242/dev.109892

Centanin, L., Hoeckendorf, B., & Wittbrodt, J. (2011). Fate restriction and multipotency in retinal stem cells. *Cell Stem Cell*, *9*(6), 553-562. https://doi.org/10.1016/j.stem.2011.11.004

Cunningham, C. L., Martinez-Cerdeno, V., & Noctor, S. C. (2013). Microglia regulate the number of neural precursor cells in the developing cerebral cortex. *J Neurosci*, *33*(10), 4216-4233. https://doi.org/10.1523/JNEUROSCI.3441-12.2013

de Almeida, M. M. A., Goodkey, K., & Voronova, A. (2023). Regulation of microglia function by neural stem cells. *Front Cell Neurosci*, *17*, 1130205. https://doi.org/10.3389/fncel.2023.1130205

Herbomel, P., Thisse, B., & Thisse, C. (1999). Ontogeny and behaviour of early macrophages in the zebrafish embryo. *Development*, *126*(17), 3735-3745. https://doi.org/10.1242/dev.126.17.3735

Herbomel, P., Thisse, B., & Thisse, C. (2001). Zebrafish early macrophages colonize cephalic mesenchyme and developing brain, retina, and epidermis through a M-CSF receptor-dependent invasive process. *Dev Biol*, *238*(2), 274-288. https://doi.org/10.1006/dbio.2001.0393

Hollyfield, J. G. (1971). Differential growth of the neural retina in Xenopus laevis larvae. *Dev Biol*, *24*(2), 264-286. https://doi.org/10.1016/0012-1606(71)90098-4

Huels, D. J., Bruens, L., Hodder, M. C., Cammareri, P., Campbell, A. D., Ridgway, R. A., Gay, D. M., Solar-Abboud, M., Faller, W. J., Nixon, C., Zeiger, L. B., McLaughlin, M. E., Morrissey, E., Winton, D. J., Snippert, H. J., van Rheenen, J., & Sansom, O. J. (2018). Wnt ligands influence tumour initiation by controlling the number of intestinal stem cells. *Nat Commun*, *9*(1), 1132. https://doi.org/10.1038/s41467-018-03426-2

Johns, P. R. (1977). Growth of the adult goldfish eye. III. Source of the new retinal cells. *J Comp Neurol*, *176*(3), 343-357. https://doi.org/10.1002/cne.901760304

Johns, P. R., & Easter, S. S., Jr. (1977). Growth of the adult goldfish eye. II. Increase in retinal cell number. *J Comp Neurol*, *176*(3), 331-341. https://doi.org/10.1002/cne.901760303

Jones, S. L., Wang, J., Turck, C. W., & Brown, E. J. (1998). A role for the actin-bundling protein L-plastin in the regulation of leukocyte integrin function. *Proc Natl Acad Sci U S A*, *95*(16), 9331-9336. https://doi.org/10.1073/pnas.95.16.9331

Levayer, R., Dupont, C., & Moreno, E. (2016). Tissue Crowding Induces Caspase-Dependent Competition for Space. *Curr Biol*, *26*(5), 670-677. https://doi.org/10.1016/j.cub.2015.12.072

Loosli, F., Koster, R. W., Carl, M., Krone, A., & Wittbrodt, J. (1998). Six3, a medaka homologue of the Drosophila homeobox gene sine oculis is expressed in the anterior embryonic shield and the developing eye. *Mech Dev*, *74*(1-2), 159-164. https://doi.org/10.1016/s0925-4773(98)00055-0

Lust, K., & Wittbrodt, J. (2018). Activating the regenerative potential of Muller glia cells in a regeneration deficient retina. *Elife*, *7*. https://doi.org/ARTN e32319

10.7554/eLife.32319
Nakayama, M. (2018). Macrophage Recognition of Crystals and Nanoparticles. *Front Immunol*, *9*, 103. https://doi.org/10.3389/fimmu.2018.00103
Nath, S., Martinez Santamaria, J. C., Chu, Y. H., Choi, J. S., Conforti, P., Lin, J. D., Sankowski, R., Amann, L., Galanis, C., Wu, K., Deshpande, S. S., Vlachos, A., Prinz, M., Lee, J. K., & Schachtrup, C. (2024). Interaction between subventricular zone microglia and neural stem cells impacts the neurogenic response in a mouse model of cortical ischemic stroke. *Nat Commun*, *15*(1), 9095. https://doi.org/10.1038/s41467-024-53217-1
Perez Saturnino, A., Lust, K., & Wittbrodt, J. (2018). Notch signalling patterns retinal composition by regulating atoh7 during post-embryonic growth. *Development*, *145*(21). https://doi.org/10.1242/dev.169698
Ratnayake, D., Nguyen, P. D., Rossello, F. J., Wimmer, V. C., Tan, J. L., Galvis, L. A., Julier, Z., Wood, A. J., Boudier, T., Isiaku, A. I., Berger, S., Oorschot, V., Sonntag, C., Rogers, K. L., Marcelle, C., Lieschke, G. J., Martino, M. M., Bakkers, J., & Currie, P. D. (2021). Macrophages provide a transient muscle stem cell niche via NAMPT secretion. *Nature*, *591*(7849), 281-287. https://doi.org/10.1038/s41586-021-03199-7
Ravichandran, K. S. (2011). Beginnings of a good apoptotic meal: the find-me and eat-me signaling pathways. *Immunity*, *35*(4), 445-455. https://doi.org/10.1016/j.immuni.2011.09.004
Reinhardt, R., Centanin, L., Tavhelidse, T., Inoue, D., Wittbrodt, B., Concordet, J. P., Martinez-Morales, J. R., & Wittbrodt, J. (2015). Sox2, Tlx, Gli3, and Her9 converge on Rx2 to define retinal stem cells in vivo. *EMBO J*, *34*(11), 1572-1588. https://doi.org/10.15252/embj.201490706
Rhodes, J., Hagen, A., Hsu, K., Deng, M., Liu, T. X., Look, A. T., & Kanki, J. P. (2005). Interplay of Pu.1 and Gata1 Determines Myelo-Erythroid Progenitor Cell Fate in Zebrafish. *Developmental Cell*, *8*(1), 97-108. https://doi.org/https://doi.org/10.1016/j.devcel.2004.11.014
Roh-Johnson, M., Shah, A. N., Stonick, J. A., Poudel, K. R., Kargl, J., Yang, G. H., di Martino, J., Hernandez, R. E., Gast, C. E., Zarour, L. R., Antoku, S., Houghton, A. M., Bravo-Cordero, J. J., Wong, M. H., Condeelis, J., & Moens, C. B. (2017). Macrophage-Dependent Cytoplasmic Transfer during Melanoma Invasion In Vivo. *Developmental Cell*, *43*(5), 549-562.e546. https://doi.org/https://doi.org/10.1016/j.devcel.2017.11.003
RStudio: Integrated Development Environment for R. In. (2023). Posit, Posit team. http://www.posit.co/.
Santos, A. M., Calvente, R., Tassi, M., Carrasco, M. C., Martin-Oliva, D., Marin-Teva, J. L., Navascues, J., & Cuadros, M. A. (2008). Embryonic and postnatal development of microglial cells in the mouse retina. *J Comp Neurol*, *506*(2), 224-239. https://doi.org/10.1002/cne.21538
Scott, E. W., Simon, M. C., Anastasi, J., & Singh, H. (1994). Requirement of transcription factor PU.1 in the development of multiple hematopoietic lineages. *Science*, *265*(5178), 1573-1577. https://doi.org/10.1126/science.8079170
Sigmundsdottir, H., & Butcher, E. C. (2008). Environmental cues, dendritic cells and the programming of tissue-selective lymphocyte trafficking. *Nat Immunol*, *9*(9), 981-987. https://doi.org/10.1038/ni.f.208
Sokol, C. L., & Luster, A. D. (2015). The chemokine system in innate immunity. *Cold Spring Harb Perspect Biol*, *7*(5). https://doi.org/10.1101/cshperspect.a016303

Soteriou, D., & Fuchs, Y. (2018). A matter of life and death: stem cell survival in tissue regeneration and tumour formation. *Nat Rev Cancer*, *18*(3), 187-201. https://doi.org/10.1038/nrc.2017.122

Stemmer, M., Thumberger, T., del Sol Keyer, M., Wittbrodt, J., & Mateo, J. L. (2015). CCTop: An Intuitive, Flexible and Reliable CRISPR/Cas9 Target Prediction Tool. *PLOS ONE*, *10*(4), e0124633. https://doi.org/10.1371/journal.pone.0124633

Thermes, V., Grabher, C., Ristoratore, F., Bourrat, F., Choulika, A., Wittbrodt, J., & Joly, J. S. (2002). I-SceI meganuclease mediates highly efficient transgenesis in fish. *Mech Dev*, *118*(1-2), 91-98. https://doi.org/10.1016/s0925-4773(02)00218-6

Thomas, M. A., Buelow, B. J., Nevins, A. M., Jones, S. E., Peterson, F. C., Gundry, R. L., Grayson, M. H., & Volkman, B. F. (2015). Structure-function analysis of CCL28 in the development of post-viral asthma. *J Biol Chem*, *290*(7), 4528-4536. https://doi.org/10.1074/jbc.M114.627786

Tsingos, E., Hockendorf, B., Sutterlin, T., Kirchmaier, S., Grabe, N., Centanin, L., & Wittbrodt, J. (2019). Retinal stem cells modulate proliferative parameters to coordinate post-embryonic morphogenesis in the eye of fish. *Elife*, *8*. https://doi.org/10.7554/eLife.42646

Uehara, S., Grinberg, A., Farber, J. M., & Love, P. E. (2002). A role for CCR9 in T lymphocyte development and migration. *J Immunol*, *168*(6), 2811-2819. https://doi.org/10.4049/jimmunol.168.6.2811

Villani, A., Benjaminsen, J., Moritz, C., Henke, K., Hartmann, J., Norlin, N., Richter, K., Schieber, N. L., Franke, T., Schwab, Y., & Peri, F. (2019). Clearance by Microglia Depends on Packaging of Phagosomes into a Unique Cellular Compartment. *Dev Cell*, *49*(1), 77-88 e77. https://doi.org/10.1016/j.devcel.2019.02.014

Wattrus, S. J., Smith, M. L., Rodrigues, C. P., Hagedorn, E. J., Kim, J. W., Budnik, B., & Zon, L. I. (2022). Quality assurance of hematopoietic stem cells by macrophages determines stem cell clonality. *Science*, *377*(6613), 1413-1419. https://doi.org/10.1126/science.abo4837

Wurbel, M. A., Malissen, M., Guy-Grand, D., Malissen, B., & Campbell, J. J. (2007). Impaired accumulation of antigen-specific CD8 lymphocytes in chemokine CCL25-deficient intestinal epithelium and lamina propria. *J Immunol*, *178*(12), 7598-7606. https://doi.org/10.4049/jimmunol.178.12.7598

Wurbel, M. A., Malissen, M., Guy-Grand, D., Meffre, E., Nussenzweig, M. C., Richelme, M., Carrier, A., & Malissen, B. (2001). Mice lacking the CCR9 CC-chemokine receptor show a mild impairment of early T- and B-cell development and a reduction in T-cell receptor gammadelta(+) gut intraepithelial lymphocytes. *Blood*, *98*(9), 2626-2632. https://doi.org/10.1182/blood.v98.9.2626

Zhu, X., Huang, L., Zheng, Y., Song, Y., Xu, Q., Wang, J., Si, K., Duan, S., & Gong, W. (2019). Ultrafast optical clearing method for three-dimensional imaging with cellular resolution. *Proc Natl Acad Sci U S A*, *116*(23), 11480-11489. https://doi.org/10.1073/pnas.1819583116

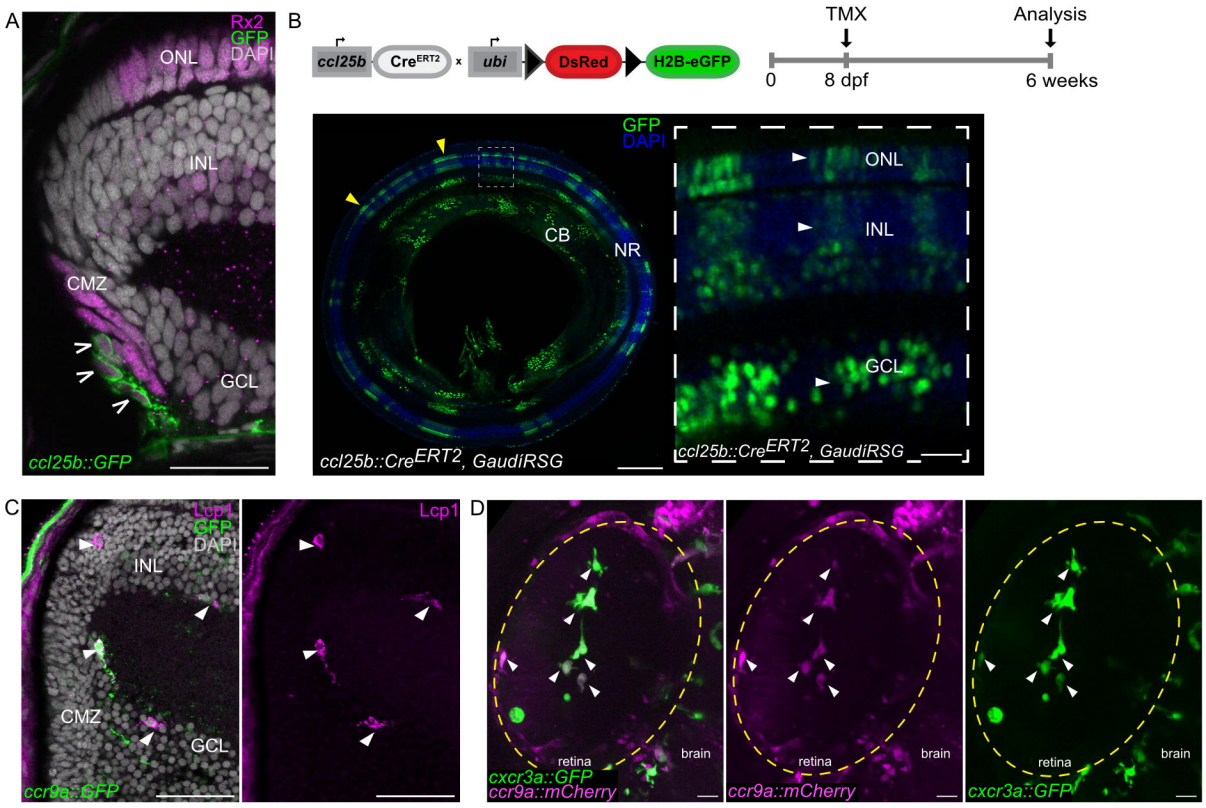
A
Rx2
GFP
DAPI
ONL
INL
CMZ
GCL
ccl25b::GFP
B
ccl25b
Cre^ERT2
x
ubi
DsRed
H2B-eGFP
TMX
Analysis
0
8 dpf
6 weeks
GFP
DAPI
CB
NR
ONL
INL
GCL
ccl25b::Cre^ERT2, GaudiRSG
ccl25b::Cre^ERT2, GaudiRSG
C
Lcp1
GFP
DAPI
INL
CMZ
GCL
ccr9a::GFP
Lcp1
D
retina
brain
cxcr3a::GFP
ccr9a::mCherry
retina
brain
ccr9a::mCherry
retina
brain
cxcr3a::GFP

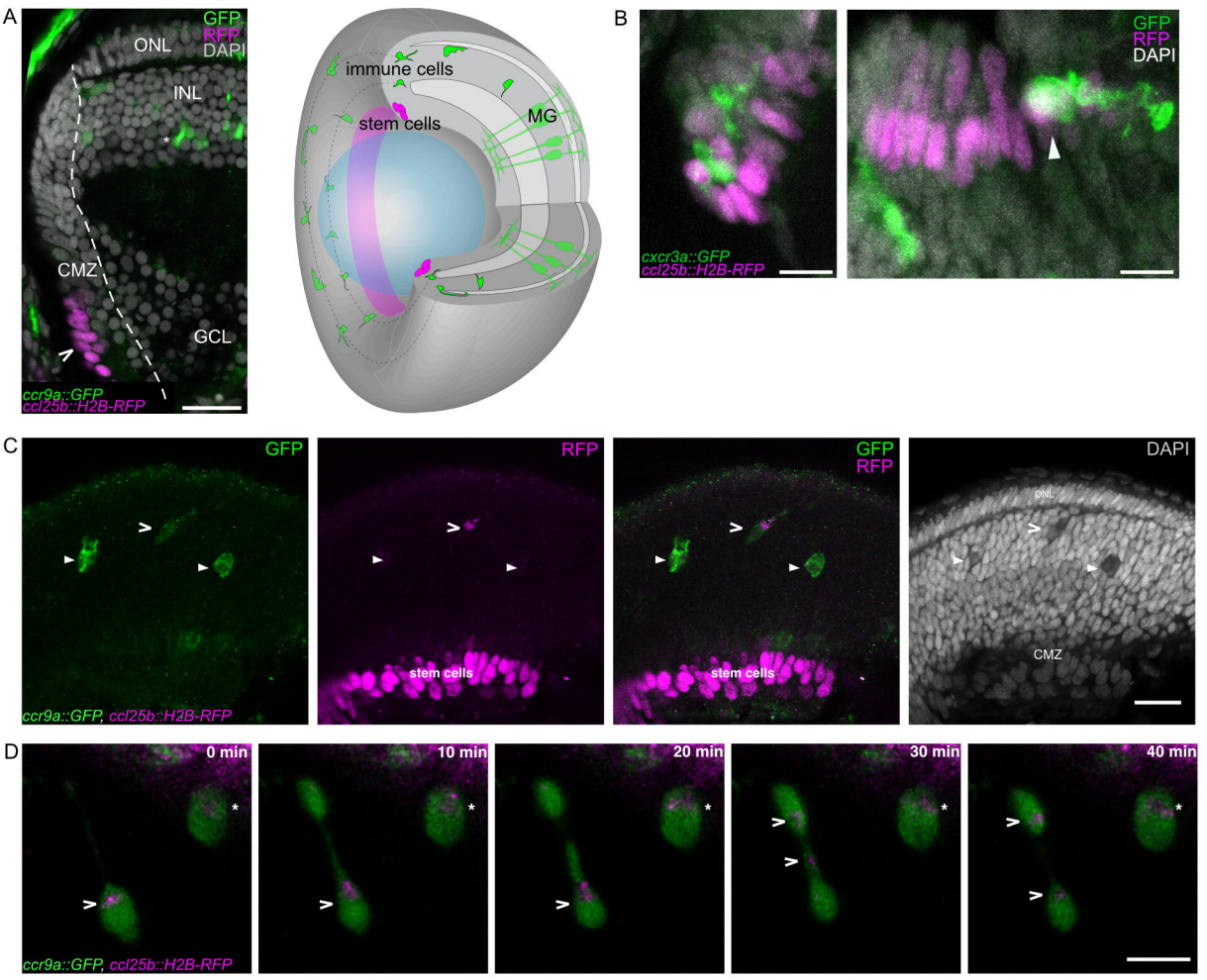
A
GFP
RFP
DAPI
ONL
INL
CMZ
GCL
ccr9a::GFP
ccl25b::H2B-RFP
immune cells
stem cells
MG
B
cxcr3a::GFP
ccl25b::H2B-RFP
GFP
RFP
DAPI
C
GFP
RFP
GFP
RFP
DAPI
stem cells
stem cells
ONL
CMZ
ccr9a::GFP, ccl25b::H2B-RFP
D
0 min
10 min
20 min
30 min
40 min
ccr9a::GFP, ccl25b::H2B-RFP

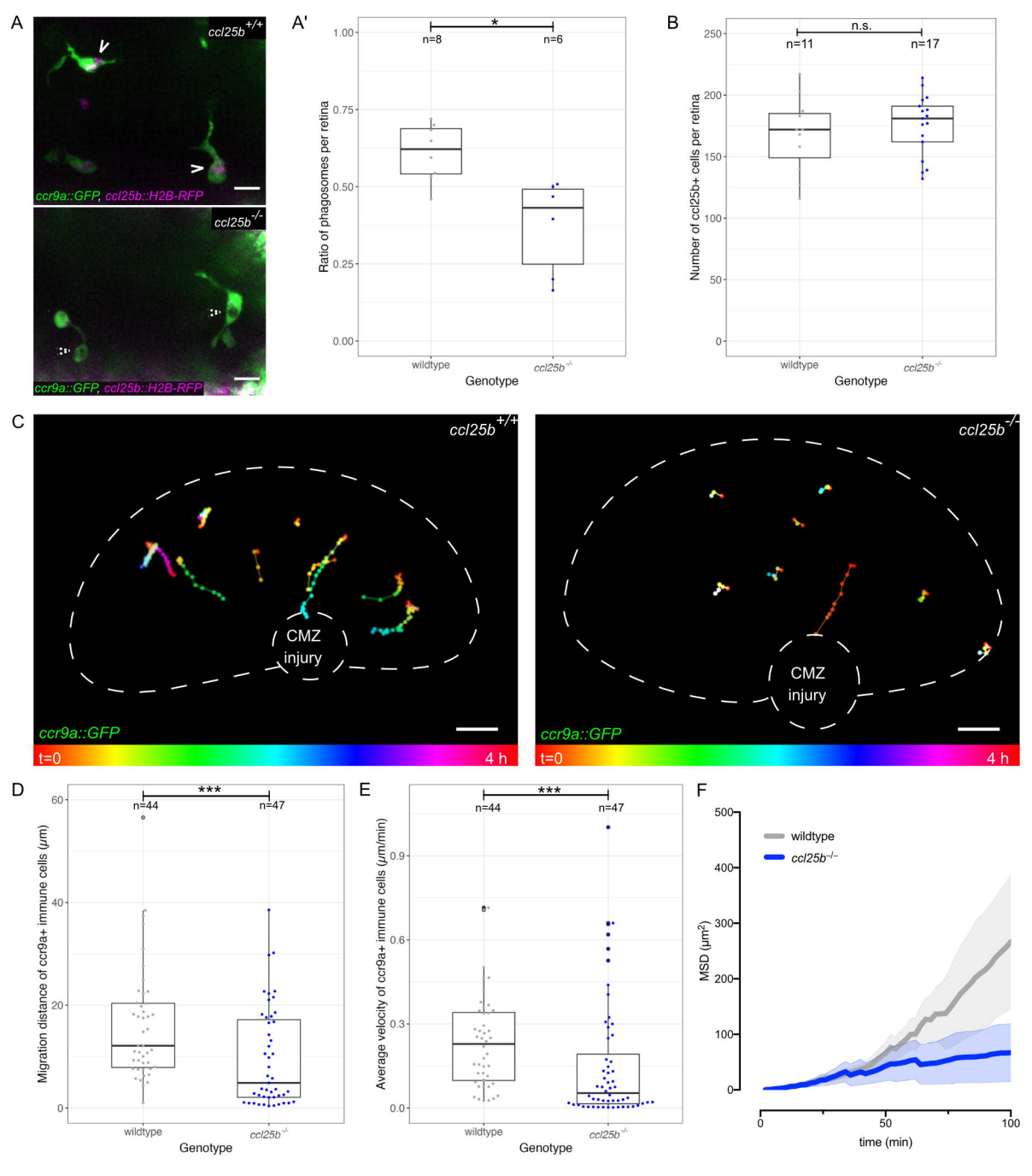
A
ccl25b+/+
ccr9a::GFP, ccl25b::H2B-RFP
ccl25b-/-
ccr9a::GFP, ccl25b::H2B-RFP
A'
*
n=8
n=6
Ratio of phagosomes per retina
1.00
0.75
0.50
0.25
0.00
wildtype
ccl25b-/-
Genotype
B
n.s.
n=11
n=17
Number of ccl25b+ cells per retina
250
200
150
100
50
0
wildtype
ccl25b-/-
Genotype
C
ccl25b+/+
CMZ
injury
ccr9a::GFP
t=0
4 h
ccl25b-/-
CMZ
injury
ccr9a::GFP
t=0
4 h
D
***
n=44
n=47
Migration distance of ccr9a+ immune cells (μm)
60
40
20
0
wildtype
ccl25b-/-
Genotype
E
***
n=44
n=47
Average velocity of ccr9a+ immune cells (μm/min)
0.9
0.6
0.3
0.0
wildtype
ccl25b-/-
Genotype
F
wildtype
ccl25b-/-
MSD (μm2)
500
400
300
200
100
0
0
50
100
time (min)

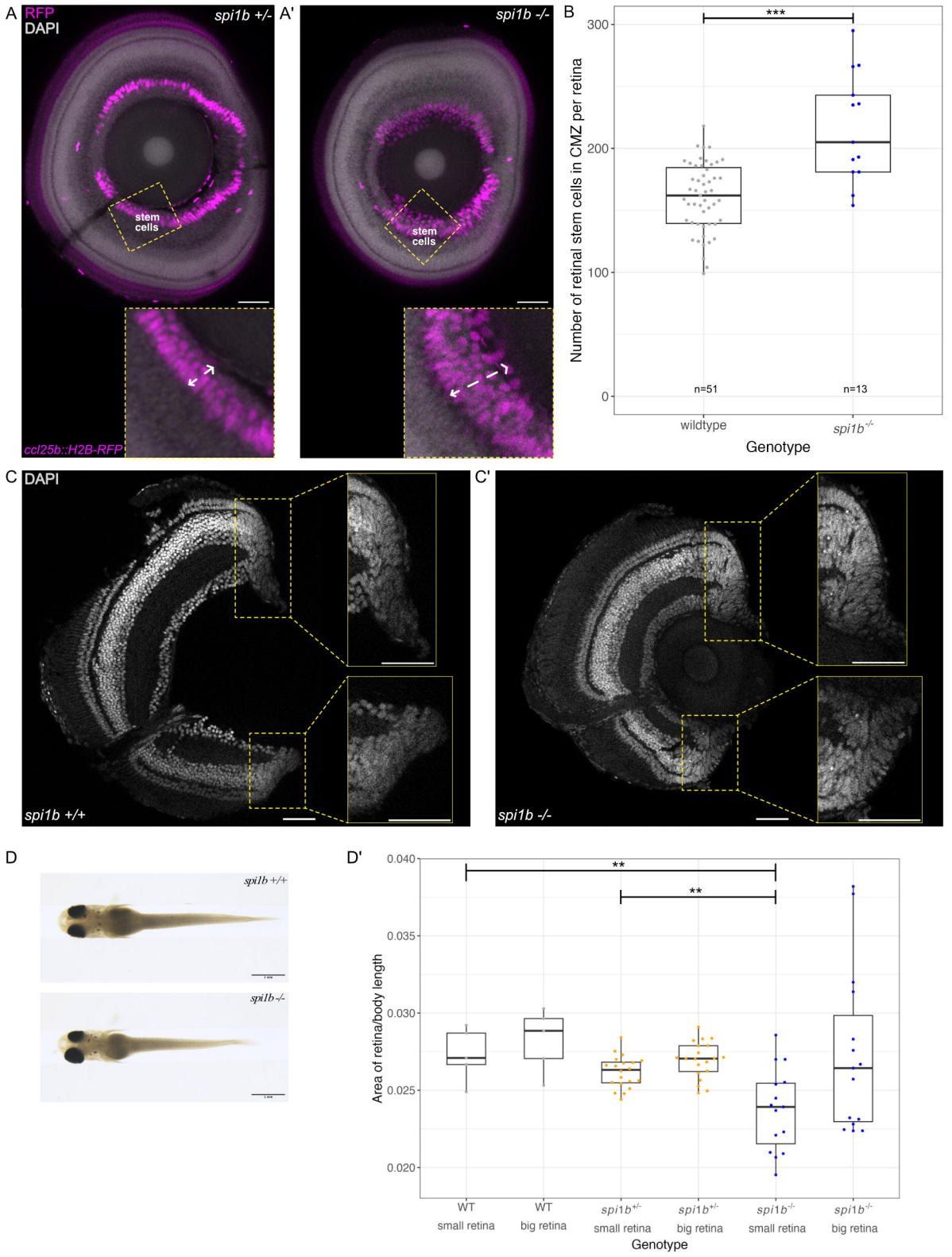
A
RFP
DAPI
spi1b +/-
stem cells
ccl25b::H2B-RFP
A'
spi1b -/-
stem cells
B
***
Number of retinal stem cells in CMZ per retina
300
200
100
0
n=51
n=13
wildtype
spi1b-/-
Genotype
C
DAPI
spi1b +/+
C'
spi1b -/-
D
spi1b +/+
spi1b -/-
D'
**
**
Area of retina/body length
0.040
0.035
0.030
0.025
0.020
WT small retina
WT big retina
spi1b+/- small retina
spi1b+/- big retina
spi1b-/- small retina
spi1b-/- big retina
Genotype